OBSERVATION OF CURRENT CONVECTIVE INSTABILITY DURING TURBULENT HEATING OF PLASMA BY A CURRENT

Yu. G. KALININ, D. N. LIN, L. I. RUDAKOV, V. D. RYUTOV, and V. A. SKORYUPIN

Submitted March 16, 1970

Zh. Eksp. Teor. Fiz. 59, 1056–1066 (October, 1970)

The results of a theoretical and experimental study of large-scale current convective instability during turbulent heating of plasma by a current are reported. A solution is given of the nonlinear equation describing the change in the longitudinal electric field in plasma, and it is shown that the current convective instability leads to a considerable increase in thermal conductivity along the magnetic field. This explains the restricted growth in the energy content of plasma and the high end losses observed experimentally.[1-3] Measurements of the electric-field distribution in plasma and of the rate of growth of perturbations are in satisfactory agreement with the theory proposed in this paper.

1. INTRODUCTION

EXISTING experimental data on turbulent heating of plasma by a current[1-3] show that the anomalous resistance of plasma and its heating are connected with the ion-acoustic current instability.[4,5] In our last paper[3] we used measurements on the electromagnetic plasma oscillations in the form of whistlers in the frequency region near $2\omega_{pi}$ to determine the intensity and spectral composition of ion-acoustic noise in the presence of anomalous resistance. The intensity W of ion-acoustic oscillations of frequency near ω_{pi} found in this way was sufficient to enable us to explain the observed effective collision frequency for the plasma electrons in terms of the formulas of the plasma turbulence theory:[4]

$$\nu_{ef} \approx \omega_{pe} W / nT_e. \tag{1}$$

The theory of ion-acoustic current instability explains the weak dependence of the ratio of the drift velocity to the ion-sound velocity on the plasma parameters, shown in Fig. 1, taken from[2].

In the ensuing analysis we shall require the voltage-current characteristic $j = j(E)$ of the plasma, which includes the ion-acoustic instability effects. The general shape of the $j(E)$ curve can be established on the basis of the following considerations.

By definition

$$j = enu = e^2 nE / m\nu_{ef}. \tag{2}$$

The quantity ν_{ef} for turbulent plasma is given by Eq. (1), whereas, in view of Eqs. (1) and (2), the drift velocity is given by

$$u = \frac{e}{m}\frac{E}{\nu_{ef}} = \frac{E}{\sqrt{8\pi nT_e}}\frac{nT_e}{W}V_{Te}. \tag{3}$$

The noise energy density W in the presence of the ion-acoustic instability under quasistationary conditions can be established from the equation

$$\frac{dW}{dt} = (\gamma_e - \gamma_i - \delta\gamma_n)W \approx$$
$$\approx \omega_{pi}\left\{\frac{u-\omega/k}{V_{Te}} - \frac{\omega}{kV_{Te}}a\left(\frac{T_i}{T_e}\right) - \frac{W}{nT_e}b\left(\frac{T_i}{T_e}\right)\right\}W \tag{4}$$

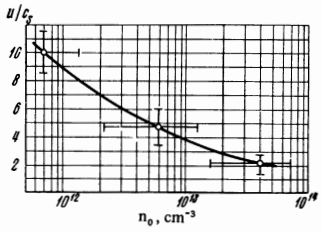

FIG. 1. Ratio u/c_S as a function of initial density.

nT, 10^{15} eV/cm³	H_0, kOe	V_{dd}, kV	n_0, 10^{13} cm⁻³	Efficiency, %
4.5			$n_0 < 0.13$	6
6.3	11	24	$0.13 < n_0 < 1.7$	8
10			$1.7 < n_0 < 7$	12
12			$7 < n_0$	15
7.7		21		13
12		28		11
20	15	33	$n_0 \sim 7$	13
27		38		13
34		45		12
4.9	5			6
9.2	7.5			11
11	11	24	$n_0 \sim 4$	14
12.5	21			15

Experimental conditions: discharge gap length l = 100 cm, radius of plasma column r = 4 cm.

which is valid when the time during which the current flows is much greater than the characteristic time $\gamma_e^{-1} \approx V_{Te}/u\omega_{pi}$ necessary for the instability development.

The first term in the above equation describes the appearance of noise following induced emission of ion-acoustic oscillations by electrons moving with ultrasonic velocity. The second term takes into account the linear damping of the oscillations by resonant ions. It depends on the structure of the ion distribution function f for $V > \omega/k$. The third term describes the nonlinear transfer of noise energy along the spectrum. For ion-acoustic oscillations the nonlinear effect, i.e., induced scattering by ions, is the principal phenomenon. The quantity $\delta\gamma_n$ may vary within certain limits, depending on the characteristic magnitude of the wave vector, the parameter T_e/T_i, and the width of the spectrum $\Delta k/k$. We have taken this into account by introducing the coefficient b.

In this way the momentum received by the electron from the electric field is successively transferred from electrons to the oscillations and from the oscillations to the ions, and a part of the dissipating energy stored in the electric field, which is equal to $\sim enEc_s$, is used to heat the main mass of the ions and the resonant plasma ions.

By solving Eq. (4) for W and substituting the result into Eqs. (2) and (3), we obtain

$$j = \omega_{pe}\frac{nT_e}{4\pi W}E =$$

$$= \frac{\omega_{pe}}{2\pi}\frac{bE}{(1+a)}\frac{V_{Te}}{\omega/k}\left[\left(1+\frac{E}{\sqrt{8\pi nT_e}}\frac{V_{Te}^2}{(\omega/k)^2}\frac{4b}{(1+a)^2}\right)^{1/2}-1\right]^{-1} \quad (5)$$

In the limit of "low" electric fields $E \ll (m/M)\sqrt{8\pi nT_e}$, we have

$$j = en(1+a)\frac{\omega}{k}\left(1+\frac{E}{\sqrt{8\pi nT_e}}\frac{V_{Te}^2}{(\omega/k)^2}\frac{b}{(1+a)^2}\right),$$

$$\frac{\omega}{k} = c_s\left(1+\frac{1}{2}k^2r_D^2\right)^{-1/2}, \quad r_D = V_{Te}/\omega_{pe}, \quad a = \frac{m}{M}\frac{f_i(\omega/k)}{f_e(\omega/k)}; \quad (6)$$

where ω/k, k are the characteristic phase velocity and wave vector of the ion-acoustic oscillations, respectively, and we are assuming that $kr_D \approx 1$, $\omega/k \approx c_s$. In high fields $E \gg (m/M)\sqrt{8\pi nT_e}$ the voltage-current characteristic is[6,5]

$$j = enc_s\left[\frac{E^2b^2}{8\pi nT_e}\frac{M^2}{m^2}\right]^{1/4}. \quad (7)$$

Equations (6) and (7) can be used to explain the experimental curve shown in Fig. 1.

Experiments have shown, however, that the energy dissipated in the discharge gap while the current flows through the plasma is not wholly used to increase this energy content. In fact, direct bolometric measurements have shown that most of this energy (up to 80%) is dissipated at the end electrode (anode).[1] The table shows the final plasma pressure and heating efficiency as functions of the initial conditions.

The data shown in the table are in conflict with the energy-balance equation which takes into account only the ion-acoustic instability:

$$\frac{3}{2}\frac{dnT}{dt} = enuE - \frac{1}{r^2}\frac{\partial}{\partial r}r^2\frac{V_{Te}^2}{\omega_{He}^2}\nu_{ef}\frac{\partial nT_e}{\partial r} -$$

$$-n\frac{\partial}{\partial z}\frac{V_{Te}^2}{\nu_{ef}}\frac{\partial T_e}{\partial z} - u\frac{\partial nT}{\partial z}. \quad (8)$$

The above values of the parameters correspond to $\nu_{ef} \lesssim 10^{10}$. The time to establish maximum nT is 0.2–0.3 μsec. Losses due to radial diffusion [second term on the right-hand side of Eq. (8)] and the transport of energy by the current electrons (fourth term) can be neglected during this time. If we substitute $\nu_{ef} = eE_z/mu$ into the third term we find that the energy losses due to thermal conduction along the magnetic field are small in comparison with the rate of heating for eEL > T. However, according to the table, this condition is always very easily satisfied. If this is so—what is responsible for the restriction on the growth of the plasma energy content? It is natural to assume that the energy losses are a consequence of large-scale instabilities. The present paper is, in fact, devoted to the theoretical analysis and experimental observation of such instabilities.

2. THEORY OF CURRENT CONVECTIVE INSTABILITY OF PLASMA WITH ANOMALOUS RESISTANCE

When we analyze the stability of plasma against slow and large-scale perturbations, the small-scale ion-acoustic instability need be taken into account only in the collision frequency. Next, under the conditions of our experiments the mean free path V_{Te}/ν_{ef} of the particles is smaller by at least an order of magnitude than the length L of the system. The macroscopic description is therefore valid. It is well known from the theory of hot laminar plasma that when eEL > T the current convective instability has the largest growth rate.[7] We shall confine our attention to this particular type of instability, assuming that the voltage-current characteristic is of the form described by Eq. (6).

The weak dependence of the current on the electric field leads to the fact that, if we are to conserve the current density, small perturbations of plasma density and temperature should lead to electric-field perturbations which are greater by a factor of

$$\frac{1}{\alpha} = \left(\frac{8\pi nT_e}{E^2}\right)^{1/2}\frac{M}{m}\frac{(1+a)^2}{b}$$

Therefore, $\delta E_z \sim E_z$ for $\delta n/n \sim \alpha$, so that if we consider $\alpha \ll 1$ we can restrict our attention to the linear approximation in the perturbations of n and T.

Our analysis will be based on the following set of equations linearized in δn, δT, and α:

$$\delta j = \frac{\partial j_0}{\partial n}\delta n + \frac{\partial j_0}{\partial T}\delta T + j_0\frac{\alpha}{E_0}\left[(E-E_0)+\frac{[VH]}{c}\right],$$

$$\frac{\partial \delta n}{\partial t} + \operatorname{div} n_0V_\perp = 0, \qquad Mn\frac{\partial V_\perp}{\partial t} = \frac{1}{c}[jH], \quad (9)^*$$

$$n\frac{\partial}{\partial t}\delta T_e = j_0\delta E_z - nV_r\frac{\partial T_e}{\partial r} + n\frac{\partial}{\partial z}\frac{T_eu}{e}\left(\frac{1}{E_z}-\frac{1}{E_0}\right)\frac{\partial T_e}{\partial z}.$$

As already noted, our experimental conditions are such that the transverse and longitudinal thermal conductivities are unimportant. Therefore, since we are concerned with perturbations for which the azimuthal number $k_\varphi = l/r$, and $k_z \approx \pi/L$, we have omitted these terms from Eq. (9). However, the second term on the right-hand side of this equation is retained since it may be quite large in the case of strong nonlinearity, $E_z - E_0 \ll E$.

The dispersion relation for the completely linearized set of equations ($\delta E_z \ll E$) and for perturbations of the form $\exp(\gamma t + il\varphi + ik_z z)$, assuming that $l \gg 1$, $k_r r \gg 1$, can readily be found and written in the form

$$\frac{k_zL}{2\pi} = \frac{1}{2}\frac{\gamma_0}{A} \pm \left\{\frac{1}{4}\frac{\gamma_0^2}{A^2} - \frac{\gamma^2L^2}{(2\pi)^2V_A^2}\left(1+\frac{l^2}{r^2}\frac{c^2E}{4\pi j}\frac{1}{A}\right)\right\}^{1/2},$$

$$\gamma_0 = c\frac{E}{H}\frac{lL}{2\pi r}\frac{\partial \ln j}{\partial r}, \qquad A = \left(\alpha\gamma + \frac{euE}{T_e}\frac{\partial \ln j}{\partial \ln T_e}\right). \quad (10)$$

The boundary condition on the conducting ends is E(0) = E(L) = 0. This means that (k = 1, 2, ...):

$$\left\{\frac{1}{4}\frac{\gamma_0^2}{A^2} - \frac{\gamma^2L^2}{(2\pi)^2V_A^2}\left(1+\frac{l^2}{r^2}\frac{c^2E}{4\pi j}\frac{1}{A}\right)\right\}^{1/2} = \frac{1}{2}k. \quad (11)$$

This is an equation for γ which leads to the following instability condition:

$$\gamma_0 > k\frac{euE}{T_e}\frac{\partial \ln j}{\partial \ln T_e} \quad \text{or} \quad \frac{l}{\pi}\frac{c_s^2L}{ur^2\omega_{Hi}}\left(\frac{\partial \ln j}{\partial \ln T_e}\right)^{-1} > k. \quad (12)$$

*[VH] ≡ V × H.

The second term in the curly brackets appears as a result of the possible nonpotential nature of the electric field of the perturbations. However, in our analysis of instabilities we shall assume that the electric field is almost potential, but in order to ensure that E_φ is zero at the ends, this perturbation must be augmented by an Alfven wave:

$$E = e^{il\varphi+\nu t}. \tag{13}$$

In this case, we can readily obtain one nonlinear equation for E_Z which we shall write in the dimensionless form

$$\frac{\partial^2}{\partial\tau\,\partial\zeta}E - \frac{\partial E}{l\,\partial\varphi} = \beta\frac{\partial^2}{\partial\zeta^2}\frac{1}{E},$$
$$E = \frac{E_z}{E_0}, \quad \tau = \frac{\gamma_0 t}{ak}, \quad \zeta = k\frac{2\pi z}{L}, \quad \beta = \frac{\partial \ln j}{\partial T_e}\frac{\partial T_e}{\partial z}\frac{Tu2\pi k^2}{eE_0\gamma_0 L}. \tag{14}$$

In the linear approximation this results in the unstable solutions

$$\gamma = c\frac{E}{H}\frac{Ll}{\pi kr}\frac{\partial \ln j}{\partial r}\left(\frac{\partial \ln j}{\partial \ln E}\right)^{-1}. \tag{15}$$

We are assuming, for simplicity, that $T(z) = T_0 + |z - \frac{1}{2}L|\,\partial T/\partial z$. The parameter β is the ratio of the energy losses due to thermal conduction to the rate of plasma heating, and is small in our experiment.

For $E \gg \beta$ the last term in Eq. (14) can be omitted. Its solution is, therefore,

$$E_1 = 1 - \psi(\zeta + l\varphi)e^{\tau}, \tag{16}$$

where ψ is the initial perturbation. For $E \ll 1$ we can seek E in the form $E = E(\xi, \tau)$, $\xi = \zeta + l\varphi$. We then have

$$\frac{\partial}{\partial\tau}E - E + 1 = \beta\frac{\partial}{\partial\xi}\frac{1}{E}. \tag{17}$$

This equation has the following solution:

$$E_2 = \left[\frac{\xi - \xi_0(\tau)}{\beta} + \chi(\tau)\right]^{-1}(1 + o(E)). \tag{18}$$

where the functions $\xi_0(\tau)$ and $\chi(\tau)$ are joined by observing the following two conditions:

These two solutions can be joined in the region where $\beta \ll E \ll 1$. This is defined by

$$E_1 = E_2, \quad 1 - \psi(\xi_0)e^{\nu\tau} = \frac{1}{\chi(\tau)},$$
$$\frac{\partial E_1}{\partial\xi} = \frac{\partial E_2}{\partial\xi}, \quad -\frac{\partial\psi}{\partial\xi_0}e^{\nu\tau} = -\frac{1}{\beta\chi^2(\tau)}. \tag{19}$$

Since by hypothesis $E_2 \ll 1$ we have $\chi(\tau) \gg 1$ and, therefore,

$$\psi(\xi_0) = e^{-\nu\tau}, \quad \chi(\tau) = \left(\beta\frac{\partial \ln\psi}{\partial\xi_0}\right)^{-1/2}.$$

Thus, finally,

$$E_2 = \left[\frac{\xi - \xi_0}{\beta} + \left(\beta\frac{\partial \ln\psi}{\partial\xi_0}\right)^{-1/2}\right]^{-1}. \tag{20}$$

As an example, consider the case where $\psi(\xi_0) = \psi_0\cos\xi_0$. So long as $t < \gamma^{-1}\ln\psi_0^{-1}$, the electric field varies linearly. Subsequently, for values of ξ for which $\cos\xi_0 \leq \psi_0^{-1}e^{-\gamma t}$, the linear theory is valid as before, whereas for $\cos\xi_0 \geq \psi_0^{-1}e^{-\gamma t}$ the electric field is described by Eq. (20) and is small for a time $t \approx 1/\gamma$ ($E \sim \beta$). This process is illustrated in Fig. 2.

During the nonlinear stage the heat flow to the ends becomes large. Although the plasma density and temperature on a given line of force vary due to radial displacements, the current is kept constant for low E because ν_{ef} is small and the surplus heat is disposed of at the ends, as a result of high thermal conductivity. The change in temperature during the time $1/\gamma$ is given by $\delta T/T \approx \delta n/n \approx \alpha$, since

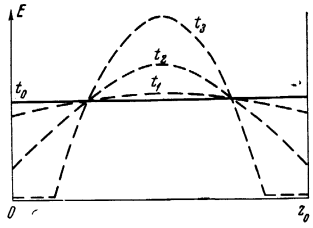

FIG. 2. Longitudinal electric field in plasma at different instants of time.

$$dT/dt \approx -\gamma\alpha T \approx -\gamma_0 T. \tag{21}$$

According to the instability criterion given by Eq. (12), these losses are always greater than the rate of heating eEu. The plasma temperature therefore falls down to a value given by

$$nT = \max\left\{\frac{E^2}{8\pi}\left(\frac{M}{m}\right)^2\frac{(1+a)^4}{b^2}, \frac{r^2eHun}{cL}\right\}. \tag{22}$$

When $nT < (E^2/8\pi)(M/m)^2(1 + a)^{-4}b^2$ the parameter α is of the order of unity, and nonlinearities in the macroscopic equations of motion restrict the fluctuation amplitude $\delta E_2/E_Z < 1$ so that the above loss mechanism becomes unimportant.

The condition given by Eq. (22) explains the experimental results shown in the table. It gives the correct relation $nT \sim V_{dd}^2$, where V_{dd} is the voltage across the direct discharge capacitance. Numerical agreement is obtained by assuming $a \approx 1$, $b \approx 1$. This choice of coefficients can be justified by comparing u/c given in Fig. 1 with the formula given by Eq. (5) for the numerical values given in the table.

We note that Eq. (22) enables us to express the conductivity of the discharge gap, σ, under the conditions of developed current-convective instability in terms of a single parameter, namely, the density: $\sigma = ne^2/m\omega_{pi}$. This is in good agreement with the experimental data (see[2]).

EXPERIMENTAL RESULTS

The experimental part of this research was carried out on the NPR-2 installation described in[1]. In[1] and in the subsequent papers[2,3] we reported a detailed study of the distribution of energy losses during turbulent heating of plasma by a current in the direct discharge, and the mechanism responsible for the turbulent heating. It was established experimentally that the process of turbulent heating has two characteristic stages in a broad range of initial conditions (magnetic field H_0 between 5 and 25 kOe, density n_0 between 10^{12} and 10^{14} cm^{-3}, initial voltage across the direct-discharge capacitance V_{dd} between 16 and 50 kV).

The first stage begins when the direct-discharge current is turned on, and is characterized by a high rate of growth of the plasma energy content U_T. It persists for 0.2—0.4 μsec during which time the thermal energy density of the plasma increases to $0.4 \times 10^{16} - 4 \times 10^{16}$ eV/cm^3, depending on the experimental conditions.

During this first stage no appreciable changes in the plasma density, and no redistribution of current over the cross section of the plasma, were observed. The resistance R_0 of the discharge circuit increases rapidly as soon as the discharge is turned on. This occurs in a time $t_0 \leq 0.05$ μsec during which the resistance rises from a low value up to a level at which it remains practically constant for the duration of the first stage. The latter value lies between 0.8 and 5.0 Ω and varies in inverse proportion to $\sqrt{n_0}$, but is independent of the magnetic field (see[2]). During the first stage there is relatively little intrinsic plasma radiation and x-ray emission from the discharge anode, which indicates the absence of high-intensity Langmuir oscillations and beams of accelerated particles with energies in excess of 1 keV during this period.

The experimental results summarized in the Introduction refer to this first heating phase of the discharge. These results lead us to the conclusion that the anomalous resistance, the high rate of absorption of energy, and the rapid heating of plasma during the first stage of the discharge are consequences of the ion-acoustic instability.

The next stage of the discharge is accompanied by rapid changes in the plasma density and the current distribution over the cross section, indicating the presence of large-scale plasma motions during this period. At the same time, there are low-frequency fluctuations in the longitudinal and azimuthal magnetic field. Strong x-ray emission appears at the discharge anode. The energy of the x rays corresponds to the order of magnitude of the applied voltage, and the intensity to a particle current at the anode which is equal to about 10% of the total discharge current. At the same time, the power radiated by the plasma into the frequency region between ω_{pe} and $2\omega_{pe}$ increase by several orders of magnitude.

The rate of energy absorption in the plasma gap during the second stage of the discharge is also high, although there is practically no heating of plasma during this period. The energy absorbed by the discharge is transported by the plasma particles along the lines of force, largely in the direction of the anode. Examination of the x-rays from the anode shows that only a small fraction of this energy is transported to the anode by the accelerated particles. The radial losses of energy which is dissipated at the ends are also increased as soon as the second stage of the discharge begins.

We must therefore conclude that, with the given initial plasma parameters, there is always a definite limit beyond which the plasma energy content cannot increase under the given condition (see the table).

To verify the extent to which this restriction on the heating is connected with the current-convective instability, we have investigated the fluctuations in the longitudinal and azimuthal electric fields.

The electric field distribution along the plasma column was obtained for different instants of time by investigating the potential difference between the grounded end (anode) and the movable electrode in the plasma as a function of distance between them. The movable electrode was a metal plate, 0.3 cm^2 in area, placed at a distance of 3 cm from the axis of the plasma column. The potential of the collecting electrode could be quite high (of the order of the applied potential difference) and, therefore, the signal had to be divided. This was achieved with the aid of a high-voltage potential divider with a total resistance $R_p = 5000$ Ω. The divider was located inside the chamber at the end of a long glass tube, 0.5 cm in diameter, which was introduced through the end at a distance of 4.5 cm from the axis of the plasma column. The potential divider was shielded and screened from possible breakdown of the glass envelope whose external diameter was 0.6 cm. The length of the divider was 12 cm. The collecting electrode was connected to the high-voltage end of the potential divider by a short wire placed in a glass capillary, 0.1 cm in diameter. The signal from the divider was fed into a 75 Ω matched cable lying inside a glass tube, and was applied to the plates of an oscillograph. The transmission band of the system was determined experimentally to be in excess of 10 MHz.

Let us now consider the interpretation of the probe signal. In our experiments the probe current I_p was considerably smaller than the ion saturation current I_i (this condition was satisfied because R_p was high). There was therefore practically no electron depletion in the neighboring plasma, and the probe collection region along the magnetic field was of the order of the electron mean free path λ. The probe could not resolve a change in the potential over a length λ. However, under our experimental conditions, the measured effective collision frequency varied between 0.8×10^9 and 5×10^9 sec^{-1} and the mean free path λ was not greater than 1 cm.

When $I_p \ll I_i$ the probe potential may differ from the plasma potential by the amount $\sim T_e/e$. Consequently, the potential $\epsilon(z_0)$ measured by the probe at the point z_0 in the column may be written in the form

$$\varepsilon \approx -\left(\int_0^{z_0} E_z\,dz + \frac{T_e}{e} + \frac{\partial \Phi}{\partial t}\right).$$

(we measured the potential relative to the anode). In this expression $E_z = j/\sigma$ is the longitudinal electric field connected with the existence of the anomalous conductivity σ and Φ is the flux of the azimuthal magnetic field of the discharge current which cuts the loop formed by the probe circuit. The flux Φ is proportional to the discharge current I. The proportionality factor L_p depends on time if the current density distribution across the column does not remain constant. Therefore, in general

$$\varepsilon = -(RI + T_e/e + L_p \partial I/\partial t + I \partial L_s/\partial t).$$

where

$$RI = \int_0^{z_0} E_z\,dz.$$

There is direct interest in evaluating this quantity.

Measurements of the distribution of the magnetic field due to the current[2] have shown that during the first stage of the discharge, which continues for about 0.3 μsec when $n_0 = 2 \times 10^{13}$ cm^{-3}, the current configuration is stable. During this time $\partial L_p/\partial t = 0$ and the ohmic part of the potential difference RI can be calculated from

$$RI = T_e/e - L_p \partial I/\partial t - \varepsilon.$$

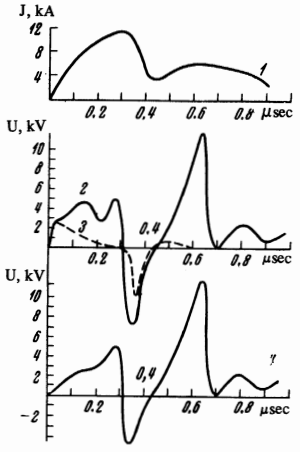

FIG. 3

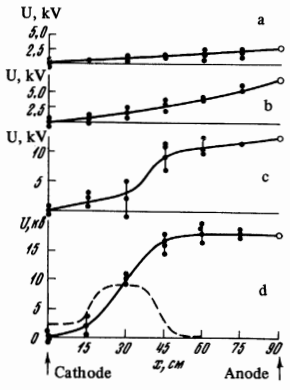

FIG. 4

FIG. 3. Analysis of probe-signal oscillograms. Curve 1—current through plasma, 2—probe potential, 3—normalized current derivative, 4—difference between curves 3 and 2.

FIG. 4. Potential distribution along plasma column at different times. The time is measured from the beginning of the discharge: a) t = 0.1 μsec; b) t = 0.2 μsec; c) t = 0.3 μsec. The broken curve shows the electric field in relative units.

The quantity L_p can be determined by using the values of the derivative of the current and the voltage drop ϵ_0 at the time when the discharge is turned on and the ohmic component is zero.

The data given in[2] show that, during the second discharge stage, there is a considerable redistribution of the discharge current which appears as a rapid increase in the current density in the axial part of the column. The term $\partial L_p/\partial t$ must be taken into account during this stage. Measurements of the magnetic field due to the current show that, for the observed time scales of the probe-potential fluctuations, the derivative $\partial L_p/\partial t$ does not exceed 0.5 Ω.

Figure 3 illustrates the processing of the probe data. Curve 2 represents the oscillogram of the probe signal with the probe at the mid-point between the electrodes (z_0 = 45 cm), the initial conditions being $n_0 \approx 2 \times 10^{13}$ cm^{-3}, V_{dd} = 23 kV, H_0 = 8 kOe. The oscillogram shows the potential drop ϵ_0 when the current is turned on. The calculated result is L_p = 43 cm. Curve 4 represents the difference between the probe potential and the quantity $L_p \partial I/\partial t$ (curve 3). During the first stage of the discharge, which continues for about 0.3 μsec, this curve gives the true value of RI (the term $\sim T_e/e$ amounts to not more than 100—500 V and can be neglected in comparison with RI).

The estimated value of $I\partial L_p/\partial t$ during the second stage of the discharge leads us to the conclusion that during the period between 0.3 and 0.5 μsec the ohmic part of the voltage (for the given probe position) is nearly zero. During the next period of time there is a considerable rise in this quantity.

We have obtained a series of results for RI as a function of time for different distances between the probe and the grounded electrode (anode). The experimental conditions were kept constant. These results were used to construct the distribution of RI along the plasma column at different instants of time (Fig. 4).

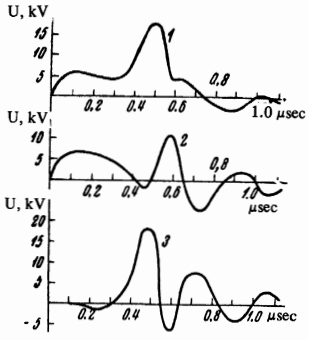

FIG. 5. Analysis of oscillograms representing signals from the two probes. Curve 1—potential on the first probe. 2—potential on the second probe, 3—potential difference between the probes as a function of time.

The derivative $\partial(RI)/\partial z$ represents the plasma electric field E_z.

Inspection of Fig. 4 will show that, at a time of the order of 0.2—0.3 μsec after the electric field is turned on, the electric field distribution in the plasma is practically uniform. This shows that there is relatively uniform energy absorption along the plasma column during the initial stage of the discharge. Our measurements enable us to estimate the total resistance of the plasma column and the energy dissipated in the plasma. The plasma resistance R_{pl} during the first stage of the discharge lay between 0.4 and 0.6 Ω under our conditions, and the total energy absorbed within the plasma during the time t_0 = 0.3 μsec from the beginning of the process was $\int_0^{t_0} R_{pl} I^2 dt$ = 12 J. It was shown in[2] that the plasma energy content in the transverse degrees of freedom, measured with the diamagnetic probe under similar experimental conditions, was 6 J. If we add to this the longitudinal energy of the particles which, under the conditions of frequent collisions, should be equal to half the transverse energy, we must conclude that practically all the energy is expended in heating the plasma during the first stage of the discharge.

After a period of 0.3 μsec measured from the beginning of the process we observe the appearance of the rapidly increasing, strong electric-field perturbations in the central part of the plasma column. These perturbations appear at the same time at which we observe the end of the increase in the plasma energy content. The character of the perturbation of the longitudinal electric field is in good agreement with the picture deduced as a result of our theoretical analysis of current-convective instability (Fig. 2).

The aim of the subsequent experiments was to investigate the azimuthal electric field which, according to the theory, accompany the current-convective instability. The azimuthal electric field was measured with two electric probes similar to the probe described above. The collecting electrodes of the probes were located within the central part of the plasma column, at 45 cm from the grounded electrode (anode) and 3 cm from the axis of the column. The azimuthal angle between the probes was 90°.

Figure 5 shows the oscillograms of signals from both probes and the difference between them which characterizes the perturbation of the azimuthal field. The experimental conditions were similar to those described above. It is clear that the potential difference between the probes is initially zero but, after a

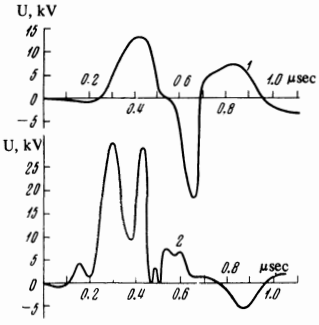

FIG. 6. Potential difference U between the probes as a function of time for different initial potential differences across the capacitor: 1) V_{dd} = 22 kV; 2) V_{dd} = 35 kV.

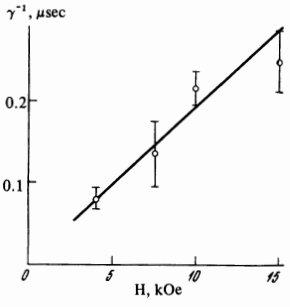

FIG. 7. Reciprocal of the growth rate of current-convective instability as a function of the magnetic field. The points represent measured rate of growth of the azimuthal electric field in plasma. $n_0 \approx 4 \times 10^{13}$ cm^{-3}; V_{dd} = 23 kV.

period of about 0.3 μsec following the beginning of the process, i.e., simultaneously with the appearance of the perturbation in the longitudinal electric field, a large potential difference between the probe was observed. This indicated the presence of a substantial azimuthal electric field in the plasma during the second stage of the discharge. The phase shift of the potential difference between the probes shows that the observed potential drop along the plasma column is not a virtual-cathode type effect but a consequence of the development of the large-scale plasma instability.

We have used our measurement data to estimate the rate of growth of the instability under different initial conditions. Figure 6 shows the azimuthal electric field for two different voltages across the direct-discharge capacitor as a function of time. It is clear that the rate of increase of the field increases with the potential difference across the capacitor. Figure 7 shows a series of values of the characteristic time scale for the growth of the perturbation as a function of the magnetic field. For comparison, the figure also shows the theoretical curve representing the reciprocal of the growth rate of the current-convective instability calculated from Eq. (15) as a function of the magnetic field. When we calculated the growth rate, we assumed that the electric field in the plasma was 0.3 esu and $l = 2$. As can be seen, there is good agreement with the theoretical predictions for the current convective instability.

[1] Yu. G. Kalinin, L. N. Lin, V. D. Ryutov, and V. A. Skoryupin, Zh. Eksp. Teor. Fiz. **56**, 462 (1969) [Sov. Phys.-JETP **29**, 252 (1969)].

[2] Yu. G. Kalinin, A. S. Kingsep, D. N. Lin, V. D. Ryutov, and V. A. Skoryupin, Zh. Eksp. Teor. Fiz. **58**, (1970) [Sov. Phys.-JETP **31**, 38 (1970)].

[3] Yu. G. Kalinin, D. N. Lin, L. I. Rudakov, V. D. Ryutov, and V. A. Skoryupin, Dokl. Akad. Nauk SSSR **189**, 2 (1969) [Sov. Phys.-Doklady **14**, 1074 (1970)].

[4] L. I. Rudakov and L. V. Korablev, Zh. Eksp. Teor. Fiz. **50**, 220 (1966) [Sov. Phys.-JETP **23**, 145 (1966)].

[5] E. K. Zavoĭskiĭ and L. I. Rudakov, Atomnaya energiya **23**, 417 (1967).

[6] R. Z. Sagdeev and A. A. Galeev, Trieste Paper IC/66/64, 1966.

[7] B. B. Kadomtsev, Collection: Voprosy teorii plazmy (Problems in Plasma Theory), Vol. 4, Atomizdat, 1964.

Translated by S. Chomet
122